Relaxation Time of Memorial Diffusion by Chronoamperometry at a Twin-electrode

ARTICLE *in* THE JOURNAL OF PHYSICAL CHEMISTRY C · OCTOBER 2007

Impact Factor: 4.77 · DOI: 10.1021/jp071757g

2 AUTHORS, INCLUDING:

Koichi Aoki
University of Fukui
171 PUBLICATIONS **3,272** CITATIONS

SEE PROFILE

Relaxation Time of Memorial Diffusion by Chronoamperometry at a Twin-electrode

Koichi Aoki* and Chaoyao Xiang

Department of Applied Physics, University of Fukui, 3-9-1 Bunkyo, Fukui-shi, 910-8507 Japan

Received: March 4, 2007; In Final Form: August 11, 2007

The diffusion flux is known to be delayed owing to a finite propagation speed, called the memory effect or the second sound for thermal diffusivity. The delay was evaluated electrochemically at a closed-spaced twin-electrode from the transient current of the ferricinium ion, which was transported by diffusion toward the other facing electrode. The traveling period, t_p, from the one electrode to the other was obtained at various separations, w, between the two electrodes. The square-root of t_p was linear with w, exhibiting an intercept. It is the intercept that reflects the memory effect. The diffusion equation with the memory, $\tau(\partial^2 c/\partial t^2) + \partial c/\partial t = D(\partial^2 c/\partial x^2)$, was solved analytically for potential step experiments to yield expressions for currents at the two electrodes, where τ is the relaxation time for the memory effect and D is the diffusion coefficient. The propagation period was expressed as $t_p^{1/2} = 0.20wD^{-1/2} + 0.764\tau^{1/2}$. Applying the data of t_p versus w allowed us to evaluate τ to be of the order of 1 ms. Values of τ decreased with an increase in concentrations of ferrocene, suggesting a participation in interaction between the redox molecules. The propagation speed defined by $(D/\tau)^{1/2}$ was 0.03 cm s^{-1}. Electrochemical responses shorter than τ may be controlled by the finite propagation speed rather than electron-transfer rates.

1. Introduction

Diffusion is a dispersion process caused by relaxation of concentration gradient. It carries a large amount of substance slowly to a macroscopic distance, whereas it transports a small amount of the substance at high speed to a microscopic length. We consider an example in which a crystal of 1 mol KCl is put into water. The solution very close to the crystal surface is saturated with K^+ and Cl^-, which diffuse into water. The probability of finding one ion at location x from the crystal surface at time t is given by[1] $1/N_A = 2\pi^{-1/2}[(Dt)^{1/2}/x] \exp(-x^2/4Dt)$, where N_A is the Avogadro constant and D is the diffusion coefficient of K^+ or Cl^-. The numerical extraction from this equation yields $x/(Dt)^{1/2} = 14.4$, leading to the velocity, $u = dx/dt = 14.4[d(Dt)^{1/2}/dt] = 7.2 \times 14.4^2 D/x^2$. This gives $u = 10^{10}$ and 10^4 m s^{-1} for $x = 1$ nm and 1 μm, respectively, at $D = 10^{-5}$ cm^2 s^{-1}. These velocities are larger than the maximum velocity of the ideal gas (plasma) of Cl^-, $u_{gas} = (2RT/w_M)^{1/2} =$ 370 m s^{-1}, with molecular weight $w_M = 35.5$ g mol^{-1} at $T =$ 25 °C. Something is wrong in the diffusion equation. This discrepancy has been considered to result in the simultaneous occurrence of the flux with the gradient in the field of heat transport.[2] It has been resolved by introducing the concept of the second sound or the memory effect,[3] in which the flux is delayed from the formation of the gradient with the first-order relaxation. The concept can be applied to diffusion because heat transfer is phenomenologically very close to diffusion in the viewpoint of statistical mechanics.[4] Diffusion may also delay the relaxation time as if it might have memory.

The second sound is a quantum mechanical phenomenon in which heat transfer occurs by wave-like motion rather than the mechanism of diffusion.[5] It has been observed in liquid helium, revealed as a macroscopic quantum and hydrodynamic effect.[6] The theoretical analysis is based macroscopically on a delay of thermal flux from the gradient of temperature. It is the same as for diffusion with memory. Consequently, no microscopic force acting on a target particle in the Langevin equation has been specified yet, and hence, it is impossible in principle to carry out dynamic simulation of diffusion with memory. There are some reports on diffusion related with memory effects, including relation between the autocorrelation function with Brownian mass,[7] relaxation of rotational Brownian motion,[8] interaction with other diffusion particles,[9] and the ballistic motion of large diffusion particles at a short time.[10] However, they may not belong to the present memory effect.

The delay of diffusion can be predicted to be observed with fast electrochemical techniques such as at fast scan voltammetry, alternating current (ac) impedance methods, and pulse methods. However, electrochemical currents at short time are often controlled by sluggish electron-transfer reaction rate.[11] Since both the effects have exhibited theoretically similar behavior in current−time curves,[12] it is important to determine which process should be a possible rate-determining step. Unfortunately, no data on the delay of diffusion have been reported, to our knowledge, probably because diffusion of interest in most physicochemical processes occurs at such a long time that the delay can be neglected.

The delay ought to be observed as an extra time of propagating a front of the conventional diffusion layer. On this concept, we suggest a technique of evaluating accurately the delay by use of a closed-space twin-electrode. One electrode generates an electroactive species, which is propagated toward the other electrode by diffusion and is detected at the electrode. The period between the time of the generation and the time of the detection should be composed of the lapse of the conventional diffusion and the inherent delay time. Since the electrode potentials at both electrodes can be set in the domain of the limiting current in this method, complications such as ohmic drop and the electron-transfer rate can be neglected. This work is devoted first to the development of the theoretical expressions

* Corresponding author. Phone: +81 90 8095 1906. Fax: +81 776 27 8494. E-mail: kaoki@u-fukui.ac.jp.

10.1021/jp071757g CCC: $37.00
Published on Web 10/03/2007

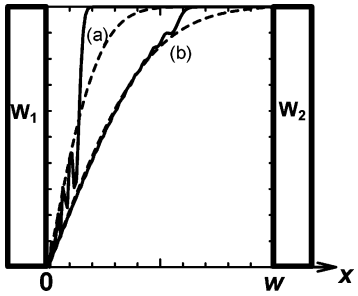

Figure 1. Model of the cell with the twin-electrode, W_1 and W_2, and concentration profiles simulated for $D\tau/w^2 =$ (solid) 0.01 and (dotted) 0.0 at $Dt/w^2 =$ (a) 0.015 and (b) 0.060.

of current−time curves at the twin-electrode including the memory effect, second to the chronoamperometric experiments at the twin-electrode with various separations, and third to the analysis of the delay of the current in order to evaluate the relaxation time of the memory.

The instrumental technique is similar to the transient scanning electrochemical microscope (SECM)[13] with the positive feedback mode,[14] in that chronoamperometric currents are observed at various distances of two electrodes. This technique is different from SECM in the electrode geometry (a tip or a plate). The aim is obviously quite different from that of SECM; the present aim is the evaluation of the delay, whereas that of SECM is drawing pattern images.

2. Theory

2.1. Derivation. The Fick's first law, $\boldsymbol{J} = -D$ grad c, expresses the occurrence of the flux, $\boldsymbol{J}$, caused by the gradient of the concentration, c, where D is the diffusion coefficient. A result is generally recognized after a delay from a cause. The occurrence of the flux (a result) may be delayed from the occurrence of the gradient (a cause). Nevertheless, the Fick's law insists on the simultaneous occurrence of the flux, $\boldsymbol{J}(t)$, at a time t and the gradient, D grad $c(t)$, at t. A diffusing particle cannot recognize the gradient by itself until it collides with at least the closest neighboring particles. This recognition period ought to delay the onset of the flux so that $\boldsymbol{J}(t + \tau) = -D$ grad $c(t)$. In other words, $\boldsymbol{J}$ tends gradually to $-D$ grad c during the period, τ, with the first-order relaxation of $\boldsymbol{J}$.[3a] When the above equation is represented as a Taylor expansion at $\tau = 0$ and the first and the second terms are retained, the relaxation of the Fick's first law can be expressed by

$$\tau(\partial \boldsymbol{J}/\partial t) = -J - D \text{ grad } c \tag{1}$$

Equation 1 is now combined with the equation for continuum:

$$\partial c/\partial t = -\text{div } \boldsymbol{J} \tag{2}$$

Carrying out the differentiation of eq 2 with respect to t, eliminating $\tau(\partial \boldsymbol{J}/\partial t)$ by use of eq 1, replacing div $\boldsymbol{J}$ by $-\partial c/\partial t$ by use of eq 2, and representing div.grad as ∇^2, we obtain

$$\tau \frac{\partial^2 c}{\partial t^2} + \frac{\partial c}{\partial t} = D\nabla^2 c \tag{3}$$

This is the Fick's second law including the memory effect. The equation for $\tau = 0$ yields the conventional Fick's second law.

A model of the electrochemical cell for measuring τ is composed of the twin-electrode in the thin layer cell with the separation, w, as is illustrated in Figure 1. The reduced species causing the electrode reaction, $R \leftrightarrow O + e^-$, is filled initially in the thin layer cell together with supporting electrolyte. It is assumed that diffusion occurs only in the x direction and that the diffusion coefficient of the oxidized species is common to that of the reduced one. When the sufficiently high oxidation potential and the sufficiently high reduction potential are applied to the left and the right electrode, respectively, the concentration of the reduced species at the left electrode is zero and that at the right electrode is kept to the initial concentration, c^*. Then the oxidized species is transported by diffusion toward the right electrode, where it is detected through the electrode reduction. This concept has been introduced in the field of the thin layer electrochemical cells.[15] Letting the concentration of the reduced species be c, we can write the initial and the boundary conditions as

$$c = c^*, \quad J = 0 \quad \text{at } t = 0 \tag{4}$$

$$c = 0 \quad \text{for } x = 0 \quad \text{at } t > 0 \tag{5}$$

$$c = c^* \quad \text{for } x = w \quad \text{at } t > 0 \tag{6}$$

Differential eq 3 includes τ but not w, whereas boundary condition 6 includes w but not τ. Consequently, τ should not vary with an experimental variable such as w but is a variable proper to the redox species.

We solve the initial and boundary value problem composed of eqs 1 and 3−6 in order to obtain expressions for the time-dependent current. The current equivalent to the flux at $x = 0$ is given by setting x to be zero in eq 1

$$\tau(\partial J_{x=0}/\partial t) = -J_{x=0} - D(\partial c/\partial x)_{x=0} \tag{7}$$

The boundary condition at $x = 0$ is expressed by this differential equation with respect to t. Carrying out the Laplace transformation of eq 7 for t, we have

$$\tau s\bar{J}_{x=0} = -D(\mathrm{d}\bar{c}/\mathrm{d}x)_{x=0} - \bar{J}_{x=0}$$

or

$$\bar{J}_{x=0} = -D(\mathrm{d}\bar{c}/\mathrm{d}x)_{x=0}/(1 + \tau s) \tag{8}$$

where the upper bar means the Laplace transformation and s is the transformed variable. The Laplace transform of eq 3 with condition 4 is given by

$$\tau(s^2\bar{c} - sc^*) + s\bar{c} - c^* = D(\mathrm{d}^2\bar{c}/\mathrm{d}x^2)$$

The solution of this equation in the finite space ($0 < x < w$) is

$$\bar{c} = c^*/s + A_1 \exp[-\sqrt{s(\tau s + 1)/D}\, x] + A_2 \exp[\sqrt{s(\tau s + 1)/D}\, x] \tag{9}$$

where A_1 and A_2 are constants. Applying the boundary conditions 5 and 6, extracting A_1 and A_2, and inserting the resulting expressions for A_1 and A_2 into eq 9, we have

$$\bar{c} = \frac{c^*}{s}\left\{1 - \frac{\exp(-\sqrt{s(\tau s + 1)/D}\, x)}{1 - \exp(-2w\sqrt{s(\tau s + 1)/D})} - \frac{\exp(\sqrt{s(\tau s + 1)/D}\, x)}{1 - \exp(2w\sqrt{s(\tau s + 1)/D})}\right\} \tag{10}$$

The current densities, j_1 and j_2, at electrodes W_1 for $x = 0$ and W_2 for $x = w$, respectively, are defined by

$$j_1 = -FJ_{x=0} \quad \text{and} \quad j_2 = FJ_{x=w} \tag{11}$$

Carrying out differentiation of eq 10 with respect to x and inserting the resulting equation into eqs 8 and 11, we obtain

$$\bar{j}_1 = \frac{Fc^*\sqrt{D}}{\sqrt{s(1+\tau s)}} \frac{1+\exp(-2w\sqrt{s(1+\tau s)/D})}{1-\exp(-2w\sqrt{s(1+\tau s)/D})} \quad (12)$$

$$\bar{j}_2 = -\frac{2Fc^*\sqrt{D}}{\sqrt{s(1+\tau s)}} \frac{1}{\exp(w\sqrt{s(1+\tau s)/D}) - \exp(-w\sqrt{s(1+\tau s)/D})} \quad (13)$$

When the exponential functions in eqs 12 and 13 are expressed in terms of the Taylor expansion for small values of $|w\sqrt{s(1+\tau s)/D}|$ and the resulting denominators are expanded around $w\sqrt{s(1+\tau s)/D} = 0$, we have

$$\bar{j}_1 = \frac{Fc^*\sqrt{D}}{\sqrt{s(1+\tau s)}} \{1 + 2\sum_{k=1}^{\infty} \exp(-2kw\sqrt{s(1+\tau s)/D})\} \quad (14)$$

$$\bar{j}_2 = -\frac{2Fc^*\sqrt{D}}{\sqrt{s(1+\tau s)}} \sum_{k=0}^{\infty} \exp(-(2k+1)w\sqrt{s(1+\tau s)/D}) \quad (15)$$

We apply the following formulas of the inverse Laplace transformation[16] to eqs 14 and 15:

$$[s(s+b)]^{-1/2} \exp(-h\sqrt{s(s+b)}) \leftrightarrow \exp(-bt/2)\, I_0((b/2)\sqrt{t^2-h^2})\, U(t-h)$$

where I_0 is the modified Bessel function of the second kind with the 0th order, and $U(x)$ is the step function ($U = 1$ for $x \geq 0$ and $U = 0$ for $x < 0$). Then we obtain

$$\frac{j_1}{Fc^*}\sqrt{\frac{\tau}{D}} = I_0\left(\frac{t}{2\tau}\right) e^{-t/2\tau} + 2\sum_{k=1}^{\infty} I_0\left(\sqrt{\frac{t^2}{4\tau^2} - \frac{k^2w^2}{D\tau}}\right) e^{-t/2\tau}\, U\left(\frac{t}{2\tau} - \frac{kw}{\sqrt{D\tau}}\right) \quad (16)$$

$$\frac{j_2}{Fc^*}\sqrt{\frac{\tau}{D}} = -2e^{-t/2\tau} \sum_{k=0}^{\infty} I_0\left(\sqrt{\frac{t^2}{4\tau^2} - \left(k+\frac{1}{2}\right)^2 \frac{w^2}{D\tau}}\right) U\left(\frac{t}{2\tau} - \frac{(k+1/2)w}{\sqrt{D\tau}}\right) \quad (17)$$

They express the dimensionless chronoamperometric curves with the parameter $w^2/D\tau$.

Since eqs 16 and 17 look divergent for $\tau \to 0$, we go back to eqs 14 and 15 in order to obtain the expressions for the chronoamperometric curves at $\tau = 0$. Applying the formulas of the inverse Laplace transformation[17]

$$s^{-1/2} \exp(-h\sqrt{s}) \leftrightarrow (1/\sqrt{\pi t}) \exp(-h^2/4t) \quad (18)$$

to eqs 14 and 15 for $\tau = 0$, the dimensionless chronoamperometric curves are given by

$$\frac{(j_1)_{\tau=0} w}{Fc^* D} = \frac{w}{\sqrt{\pi Dt}} \{1 + 2\sum_{k=1}^{\infty} \exp(-k^2w^2/Dt)\} \quad (19)$$

$$\frac{(j_2)_{\tau=0} w}{Fc^* D} = -\frac{2w}{\sqrt{\pi Dt}} \sum_{k=0}^{\infty} \exp(-(k+1/2)^2 w^2/Dt) \quad (20)$$

Equation 19 is actually the same as the expression for the chronoamperometric curve at a thin layer cell when the reverse reaction occurs at the facing electrode.[18]

2.2. Chronoamperometric Curves for $\tau = 0$. We overview the chronoamperometric curves for $\tau = 0$. The current $(j_1)_{\tau=0}$ at a short time is proportional to $t^{-1/2}$, as seen from eq 19. The Laplace-inversed current at a longer time tends to Fc^*D/ws by use of Taylor expansion of the exponential terms in eq 12. Then $(j_1)_{\tau=0} w/Fc^*D$ tends to unity for a long time. In contrast, the current $(j_2)_{\tau=0}$ at a short time is zero because of $\exp(-w^2/4Dt) \ll t^{-1/2}$ in eq 20. The Taylor expansion of the exponential terms in eq 13 for small values of $|s|$ yields $-Fc^*D/ws$. Thus, $(j_2)_{\tau=0} w/Fc^*D$ tends to -1 for $t \to \infty$.

The numerical values the chronoamperometric currents for eqs 19 and 20 were plotted in Figure 2. The current density $(j_1)_{\tau=0}$ is relaxed and approaches the steady-state value, Fc^*D/w. It becomes larger than Cottrell's current (curve c) for $Dt/w^2 > 0.3$. In contrast, the current density $(j_2)_{\tau=0}$ remains zero for $Dt/w^2 < 0.05$. It decreases and tends to $-Fc^*D/w$. The steady-state value of $(j_2)_{\tau=0}$ is compensated with that of $(j_1)_{\tau=0}$. A characteristic of the curves in the context of the propagation is the time at which $(j_2)_{\tau=0}$ begins to decrease with the time. We define the propagation time, t_p, as the dimensionless intersection, Dt_p/w^2, with the tangent line of $(j_2)_{\tau=0}$ versus t curve at the inflection point, as is shown as line d in Figure 2. The time t_p can be regarded as the period of arriving for the oxidized species at the detector electrode. According to Figure 2, it is given by

$$(D\, t_p)^{1/2} = 0.220\, w \quad (21)$$

Values of $t_p^{1/2}$ should be proportional to w if $\tau = 0$. The slope has allowed us to determine the diffusion coefficient. Equation 21 is different from the expression in which the thickness of the diffusion layer, $(\pi Dt)^{1/2}$, is equal to w ($(Dt)^{1/2} = 0.56w$). The thickness of the diffusion layer at t_p is approximately a quarter of w.

2.3. Chronoamperometric Curves for $\tau > 0$. The chronoamperometric curves for $\tau > 0$ vary with the parameter, $D\tau/w^2$. We shall predict short and long time responses for j_1 and j_2. The current of j_1 at a short time can be estimated from eq 16 by taking the leading term of eq 16 and by using the ascending series,

$$e^{-z} I_0(z) = 1 - z + 3z^2/4 - \cdots \quad (22)$$

Then we obtain

$$j_1/F = c^*\sqrt{D/\tau}(1 - t/2\tau + \cdots) \text{ at a short time} \quad (23)$$

The current of j_2 at a short time is expressed by eq 17 for $k = 0$. It is absolutely zero for $t < w\sqrt{\tau/D}$ owing to the step function rather than approximating zero like curve b in Figure 2. It begins to flow suddenly at $t = w\sqrt{\tau/D}$. This discontinuous variation is ascribed to the propagation at the constant speed, $\sqrt{D/\tau}$. In other words, the oxidation species is propagated like a soliton or a tsunami.

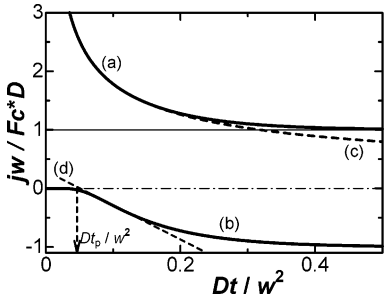

Figure 2. Dimensionless chronoamperometric curves for $\tau = 0$, calculated from eqs 19 and 20 for curves a and b, respectively. Curve c is for the Cottrell current. Line d is the tangent line at the inflection point of curve b.

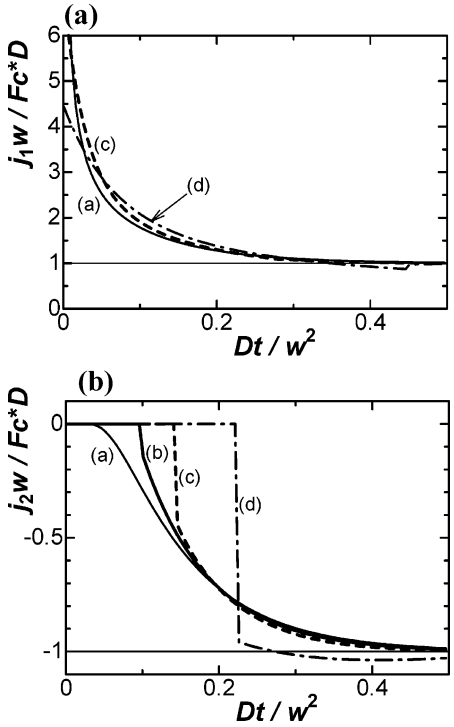

Figure 3. Dimensionless chronoamperometric curves for the oxidation (A) at the generator and the reduction (B) at the detector for $D\tau/w^2 =$ (a) 0.0, (b) 0.01, (c) 0.02, and (d) 0.05, calculated from eqs 16 and 17.

Since eqs 14 and 15 are expansions for large $|s|$ or small t, the estimation of the long term behavior requires expansions at small $|s|$ for eqs 12 and 13. The Taylor expansions of eqs 12 and 13 about $|s| = 0$ yield $Fc^*D/ws(1 + \tau s)$ and $-Fc^*D/ws(1 + \tau s)$, respectively. Their Laplace inversed forms are

$$j_1/F = (c^*D/w)(1 - e^{-t/\tau} - \cdots) \qquad \text{at a long time} \tag{24}$$

$$j_2/F = -(c^*D/w)(1 - e^{-t/\tau} - \cdots) \qquad \text{at a long time} \tag{25}$$

The time approaching the steady states delays from the case for $\tau = 0$ by the exponential term.

We computed eqs 16 and 17 for various combinations of Dt/w^2 and $D\tau/w^2$ by use of the approximate equation of the Bessel function.[19] Figure 3 shows the chronoamperometric curves of j_1 and j_2 for some values of $D\tau/w^2$. The currents, j_1, at the generator for any value of $D\tau/w^2$ decay to approach the steady state, Fc^*D/w. Values of $(j_1)_{t=0}$ for $D\tau/w^2 < 0.02$ are so large that they look like infinity on the current scale of the steady state. Those for $D\tau/w^2 > 0.05$ get to have only a few times larger magnitude than the steady-state value and hence show

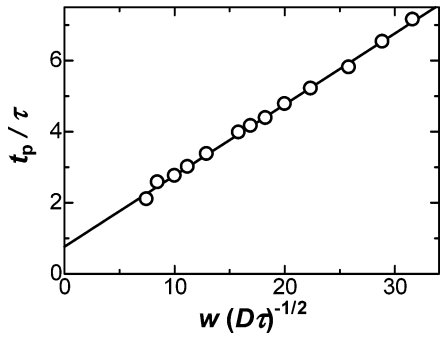

Figure 4. Variation of t_p/τ with $w(D\tau)^{-1/2}$, obtained from the graphical analysis of the curves of j_2w/Fc^*D vs Dt/w^2 computed from eq 17 for various values of $D\tau/w^2$.

the behavior as if the overall reaction might be controlled by a charge-transfer reaction rate. On the other hand, the current, j_2, decreases from zero to the steady state, $-Fc^*D/w$ with a delay. The delay increases with an increase in $D\tau/w^2$. Shape of the chronoamperometric curve becomes sharper as the value of $D\tau/w^2$ increases. The sudden variation of j_2 is ascribed to the arrival of the wave front or mathematically the step function in eq 17.

We carried out the numerical calculation of concentration profiles by use of the software modified for the present boundary conditions.[6] The computed profiles are shown in Figure 1 for $\tau > 0$ (solid) and $\tau = 0$ (dotted). The diffusion front propagates from W_1 to W_2. The delay of the front, which is represented by the difference between the solid and the dotted curve, is obvious.

The delay in j_2 is a significant feature of the propagation time. We plotted a tangent line of the chronoamperometric curves for j_2 at an inflection point and obtained the delay time, t_p, as is similar to that in Figure 2. Values of t_p/τ were plotted against Dt_p/w^2 in Figure 4, falling on the line expressed approximately by

$$\sqrt{t_p} = 0.20\, w/\sqrt{D} + 0.764\,\sqrt{\tau} \tag{26}$$

The slope of the plot of $t_p^{1/2}$ against w is slightly smaller than that in eq 21 for $\tau = 0$ because of the difference in shape of the current−time curves for $\tau > 0$ and $\tau = 0$. A value of the intercept may allow us to evaluate τ. Multiplying both hand sides by $D^{1/2}$, we obtain

$$\sqrt{Dt_p} - 0.764\,\sqrt{D\tau} = 0.20\, w \tag{27}$$

The conventional thickness of the diffusion layer, $(Dt_p)^{1/2}$, includes not only w but also the latent propagation thickness, $0.764(D\tau)^{1/2}$, by the delay.

3. Experimental Section

Working electrodes were platinum disks 1.6 mm and 0.5 mm in diameter (BAS, Tokyo). Either electrode (W_1 or W_2) was mounted in the electrochemical cell from the bottom of the cell, sealed with silicon rubber, as is illustrated in Figure 5. The other working electrode was mounted in the cell from the top so that its electrode surface was faced with the former electrode. It was supported by an *XYZ*-positioning stage, HS-3 (Melles Griot, Tokyo) with a homemade brass joint (J). The positioning stage was driven with 3 μm manually and 3 piezoelectric devices. The cell and the positioning stage were set on an optical vibration-isolating table, J01 (Suruga Seiki, Japan). The reference electrode was Ag|AgCl, and the counter electrode was platinum coil.

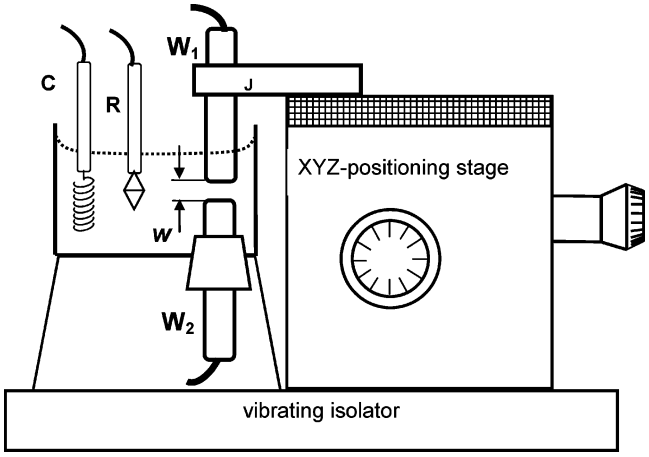

Figure 5. Illustration of the structure of the electrochemical cell and electrodes.

We attempted to use a dual potentiostat, but we observed the influence of the potential change at W_2 on current at W_1 even when the distance between the two electrodes was over 1 cm. The influence is ascribed to an electric communication at the dual potentiostat rather than the Faradaic communication. We found the use of two identical potentiostats, Potentio/Galvanostat 1112 (Huso, Kawasaki), helpful to minimize this problem. A degree of the electric communication was checked not only with a dummy cell (an electric resistance) but also with two working electrodes in a cell including ferrocene. We confirmed that only a spike of current at W_2 was observed when a potential at W_1 was stepped. Potential control and current acquisition were made through a DA/AD converter. The software was homemade.

(Ferrocenylmethyl)trimethylammonium chloride (FcTMA) was purified by sublimation. Supporting electrolyte was 1 M KCl aqueous solution. Water was distilled and ion-exchanged. Nitrogen gas was bubbled before each voltammetric run. The surfaces of the two electrodes were polished with alumina powder with attention given to keeping the surface normal to the axis of the electrode holder. The two electrodes were positioned in the solution-included cell with the positioning stage, and the *xy* position was adjusted so that the centers of the disk electrodes were closed by monitoring the optical microscope. W_1 was lowered with the *z*-positioning stage so that it was contacted with W_2. The contact was confirmed not only by an optical microscope but also by detection of equivoltage at W_1 and W_2 with a voltmeter. Location of W_1 was moved up by a given distance. The potential at W_1 was kept at the reduction potential (0.17 V vs Ag|AgCl), whereas the potential at W_2 was stepped from 0.17 V to the limiting current domain (0.50 V vs Ag|AgCl). Here, W_1 and W_2 worked as a detector and a generator, respectively. The role was exchanged by exchanging the terminal connection. Currents at a chronoamperometric curve were sampled at each 1 ms.

4. Results and Discussion

Figure 6 shows cyclic voltammograms of FcTMA at W_1 and W_2 when the potential at W_1 was scanned while the steady potential (0.17 V) was applied to W_2, where the abscissa is the potential at W_1. Current (a) at W_1 (1.6 mm in diameter) looks like a conventional voltammogram at a large electrode, of which peak potential difference was approximately 80 mV. The reaction is obviously $FcTMA^+ \leftrightarrow FcTMA^{2+} + e^-$. In contrast, the cathodic current (b) began to flow after reaching the anodic peak (a) at W_1, because $FcTMA^{2+}$ generated at W_1 reached

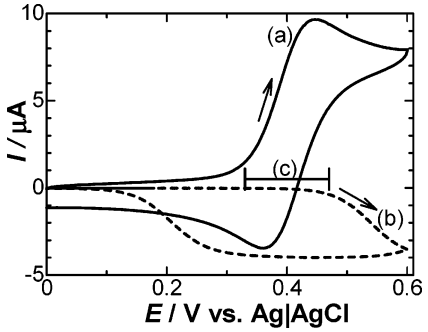

Figure 6. Cyclic voltammograms of the aqueous solution including 4 mM FcTMA and 1 M KCl at electrodes (a) W_1 1.6 mm in diameter and (b) W_2 0.5 mm in diameter when the potential of W_1 was scanned at 0.030 V s^{-1} and that of W_2 was kept at 0.17 V. The distance between two electrodes was $w = 44$ μm. Arrow c stands for the potential difference between the rising parts of currents a and b.

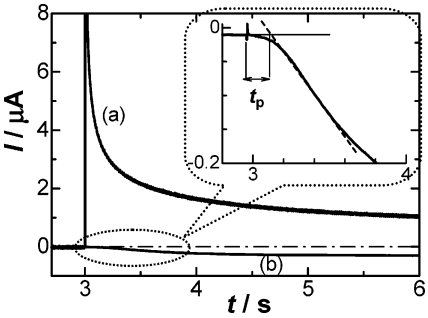

Figure 7. Chronoamperometric currents I_1 at W_1 and I_2 at W_2 when the potential of W_1 1.6 mm in diameter was stepped from 0.17 to 0.50 V at 2.9 s while that of W_2 0.5 mm in diameter was kept at 0.17 V. The inset is the magnification of a part of b.

W_2 with a delay to be reduced at W_2, like the well-known current−potential profile at a rotating disk electrode[20] and chronoamperometry at interdigitated electrodes.[21] This Faradaic interaction deforms the voltammetric shape of a and b from the conventional one. The potential difference between the raising currents of a and b was 0.14 V (arrow c), corresponding to 4.7 s. This period is of the order of the diffusion time through the two electrodes. So far, as the potential at W_1 was in the limiting current domain ($E > 0.39$ V) at the backward scan, the current b remained at the steady state, as for the redox cycling at the interdigitated array electrodes.[22] The reason for the appearance of the peaks of current a is due partially to diffusion of $FcTMA^+$ from the bulk and partially to the delay until reaching the steady state.

Figure 7 shows chronoamperometric curves at W_1 and W_2 when the potential of W_1 was stepped from 0.17 to 0.50 V while that of W_2 was kept at 0.17 V. The oxidation current I_1 decayed like Cottrell's current immediately after the potential step, and approached a steady-state value rather than zero. In contrast, the current $|I_2|$ exhibited small noise by sensing the potential step noise at W_2, as is shown in the inset of Figure 7 at $t = 2.9$ s. It increased gradually and reached the steady-state value. We draw a tangent line of the curve at the inflection point and evaluated the delay period, t_p, from the intersection of the tangent line with the background current (see the inset of Figure 7). Values of t_p were larger with an increase in the separation, *w*, between the two electrodes.

Figure 8 shows the plot of $t_p^{1/2}$ against *w*, demonstrating a linear variation as is expected from eq 26. The slope gives the value of *D* to be 0.69×10^{-5} cm^2 s^{-1}. We can see a small value of the intercept, 0.023 $s^{1/2}$, in Figure 8. The standard deviation of every point from the regression line was 0.0086

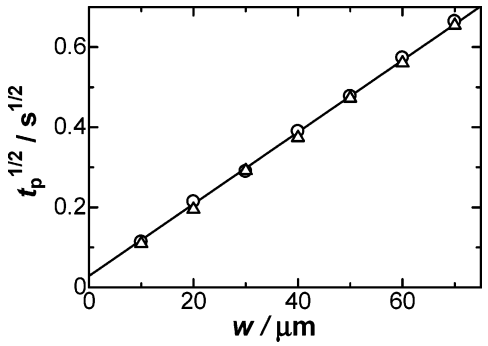

Figure 8. Variation of $t_p^{1/2}$ with w when the potential step from 0.17 to 0.50 V was applied to W_1 (circles) and W_2 (triangles) during application of the steady potential 0.17 V to W_2 (circles) and W_1 (triangles), respectively, in 2.0 mM FcTMA + 1.00 M KCl aqueous solution. The regression line has the correlation coefficient 0.9997.

TABLE 1: Variations of τ and D with Concentrations of FcTMA

[FcTMA]/mM	$D \times 10^5$ cm^2 s^{-1}	τ/ms	u/cm s^{-1}
0.5	0.75	1.05 ± 0.17	0.027
1.0	0.74	0.39 ± 0.10	0.031
2.0	0.69	0.91 ± 0.13	0.028
4.0	0.76	0.62 ± 0.05	0.038
7.0	0.63	0.05 ± 0.17	0.025
average	0.71 ± 0.06		0.030 ± 0.005

$s^{1/2}$. Therefore, the intercept value should be beyond errors and is meaningful. Inserting this value into eq 27, we obtain

$$\tau = ([\text{intercept}]/0.764)^2 = (0.91 \pm 0.13)\ \text{ms}$$

where the error denotes the standard deviation of values of t_p. We exchanged the roles of the potential control by connecting the potential-stepped terminal to W_2 and connecting the potential-constant terminal to W_1. The chronoamperometric curves depended on the terminal exchange because of the difference in size of the electrodes. However, values of t_p did not vary with the terminal exchange, as is shown in Figure 8 (comparison of circles with triangles). Therefore, values of t_p are independent not only of the size of electrodes but also of the direction of the gravity.

We carried out chronoamperometry for various concentrations of FcTMA at the twin-electrode and made plots similar to Figure 8. Values of t_p at concentrations less than 0.2 mM contained many errors owing to non-negligible electric communication between I_1 and I_2. All plots over 0.5 mM showed variations similar to Figure 8. Values of the intercept decreased with an increase in the concentration, whereas those of the slope were almost kept a constant. Table 1 shows the dependence of values of D and τ on the concentration, where the errors are their standard deviations in the plots of $t_p^{1/2}$ against w. Values of τ decreased linearly with an increase in the concentration, as is shown in Figure 9, and reached zero at [FcTMA] = 7.5 mM. The memory effect is more remarkable at lower concentrations.

Equation 3 with the condition $|\partial c/\partial t| \ll |\partial^2 c/\partial t^2|$ becomes

$$\frac{\partial^2 c}{\partial t^2} = \frac{D}{\tau}\frac{\partial^2 c}{\partial x^2} \tag{28}$$

This is a wave equation with the velocity, $u = (D/\tau)^{1/2}$, of the propagation. Values of the velocity are listed in Table 1. The average value, 0.03 cm s^{-1}, is indicative of possible participation in other rate-determining steps such as a heterogeneous rate constant. Rate constants with the Butler−Volmer type more than this value have been reported by means of

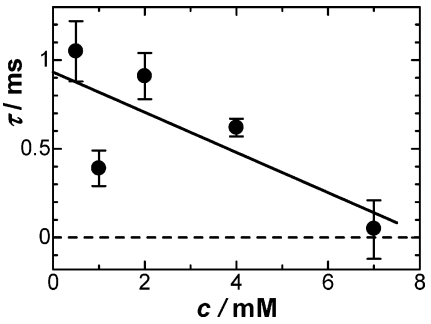

Figure 9. Dependence τ on concentrations of FcTMA.

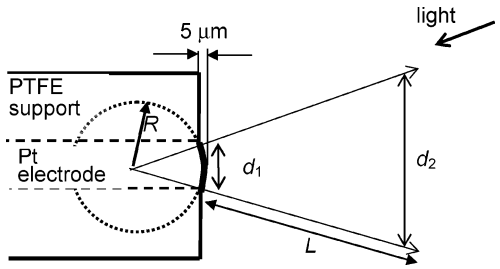

Figure 10. Illustration of the method of estimating the curvature of the electrode surface.

classically short time current transients[23]and recently ultrafast scan voltammetry as fast as 1 MV s^{-1}.[24] Since the current−time curve for the diffusion-included Butler−Volmer type is different from the curve with the memory diffusion,[5] it is possible to evaluate rate constants larger than 0.03 cm s^{-1} at the cost of accuracy.

It is significant to address errors contained in the present measurement. The variables relevant to the measurement are the bulk concentration of FcTMA, the distance between two electrodes, the time difference, and the areas of the electrodes. Both the concentration and the electrode areas are independent of the evaluation of t_p at all. The accuracy of the distance and time may be main sources of causing errors. The distance was evaluated from the vertical shift of electrode W_1 from the electrically contacting point with W_2 by means of the positioning stage with the precision 20 nm nominally. An error of the distance may arise from curvature of the electrode surface. In order to estimate the curvature, we irradiated a laser beam on the electrode surface and projected the reflecting light on a screen, as is illustrated in Figure 10. We measured the diameter (d_2) of the circular image of the reflected light and the distance (L) between the screen and the electrode. The ratio of the diameter of the electrode (d_1) to d_2 was 0.013, which should be equal to $R/(L + R)$, where R is the radius of the curvature of the electrode surface. The value of R was 60 mm for the 1.6 mm electrode, corresponding to the maximum difference 5.0 μm (= 60 mm × (1 − cos(tan^{-1} 0.013)) from the protruded part to the edge of the electrode. Consequently, a value of w read with the positioning stage is the minimum of possibly allowed values. A value of t_p may correspond to the minimum value of w because it is extrapolated to zero current or the shortest time.

The other error lies in deviation of transient current from ideal one owing to a time constant of a cell. Generally, the Cottrell equation has fitted experimental data in a limited time-domain[25] because of (i) participation of capacitive current, (ii) edge effects at electrodes by lateral diffusion, (iii) natural convention by difference in densities of electroactive species, (iv) a delay of a potentiostat, and (v) other effects including diffusion with memory.

If items i−iv were to be negligible, the relaxation time for the memory effect should be evaluated only from chronoamperometry without using the twin facing electrodes. Items i−iii underestimate the Faradaic transient current to make t_p shifted in the negative direction, whereas items iv and v overestimate the current to increase t_p. In other words, the former underestimates τ, while the latter overestimates τ. Therefore, it may be enough to examine only item iv in order to estimate the possible minimum value of τ. A delay of the potentiostat was determined by connecting an electric resistance of 100 kΩ and applying 0.1 V potential step with the current follower of a 1 MΩ resistance. The current increased at the rate of 300 μA s^{-1} to 1 μA. Since the current values effectively determining t_p were less than 0.1 μA, as is shown in the inset of Figure 7, the delay of the potentiostat was 0.3 ms. This is less than experimental errors for t_p. The other evidence that the τ values are not due to a time constant of the cell is the observation of τ only for low concentration of FcTMA (Figure 9). The time constant of the cell ought to make a larger influence on t_p with an increase in the current or an increase in a load to the potentiostat.

The instrumental concept in this work is close to that of a scanning electrochemical microscope (SECM) if a tip electrode of SCEM is replaced by such a large electrode that the linear diffusion space can be formed against the other electrode. In order to determine τ accurately, it is necessary to keep w and t_p small. However, smaller values yield larger errors owing not only to a delay of a potentiostat but also to uniformity of w. Our experience has shown that domains $10 < t_p < 500$ ms and $w > 10$ μm provided reproducible values of τ. Therefore, performance of SECM is not useful for the evaluation of τ. The value of the intercept in Figure 8, corresponding to $\tau^{1/2}$, is much smaller than $t_p^{1/2}$ (ranging from $(0.02 < (\tau/t_p)^{1/2} < 0.19)$ and can be determined only by the extrapolation in the plot of Figure 8. Consequently, the memory effect would have been neglected from experimental data that were obtained by the instruments[7−9] similar to the present work.

The dependence of τ on the concentration (Figure 9) may cause complications of the analysis of the data because τ was assumed to be independent of the concentration in the derivation of eq 8. In order to obtain the relation between τ and the concentration, this assumption is inevitable at present.

5. Conclusion

The presence of diffusion with memory was confirmed quantitatively by evaluating the relaxation time from the traveling time of the redox species at the twin-electrode. The analytical expression has demonstrated that the nonzero intercept of the plot of $t_p^{1/2}$ against w stands for the memory effect. Although values of the intercept were small in comparison with values of $t_p^{1/2}$, they are much larger than predicted errors. Therefore, they are essential and stand for the memory effect.

The short time response was measured in the one-dimensional diffusion space ($w \ll d_1$) under the limiting current conditions. Therefore, the observed values are independent of applied potentials, resistance of the solution, or size of the electrodes. They ought to depend strongly on temperature through viscosity of solvent.

The relaxation time decreased with an increase in the concentration of FcTMA. The concentration dependence suggests the participation in an interaction between diffusing molecules. For a smaller interaction or concentration, it takes more time to recognize the concentration gradient before causing the flux. Values of τ may not be inherent but depend on redox species, because they are related to the interaction between redox molecules. The propagation velocity may also vary from species to species. A theoretical approach to the relation between the recognition time and the interaction will be required to fully understand the relaxation time.

Acknowledgment. This work was financially supported by Grants-in-Aid for Scientific Research (Grants 18350041) from the Ministry of Education in Japan.

References and Notes

(1) Crank, J. *The Mathematics of diffusion*; Clarendon Press: Oxford, 1975; p 21.

(2) (a) Ulbrich, C. W. *Phys. Rev.* **1961**, *123*, 2001. (b) Vernotte, P. *Compt. Rend.* **1958**, *246*, 3154. (c) Cattaneo, C. *Compt. Rend.* **1958**, *247*, 431.

(3) (a) Chester, M. *Phys. Rev.* **1963**, *131*, 2013. (b) Load, H. W.; Shulman, Y. *J. Mech. Phys. Solids* **1967**, *15*, 299. (c) Szekeres, A. *Period. Polytech. Mech. Eng.* **2004**, *48*, 83.

(4) Kittel, C. *Thermal Physics;* John Wiley & Sons, Inc.: New York, 1969; pp 203−220.

(5) Landau, L. D.; Lifshitz, E. M. *Fluid Mechanics*; Pergamon Press: Oxford, 1987; pp 515−526.

(6) (a) Peshkov, V. *J. Phys. USSR III* **1944**, 381−382. (b) Vinen, W. F. *Proc. R. Soc. London A* **1957**, *140*, 114.

(7) Kneller, G. R.; Sutmann, G. *J. Chem. Phys.* **2004**, *120*, 1667.

(8) (a) Dejardin, P. M. *J. Mol. Liq.* **1999**, *81*, 181. (b) Blokhin, A. P.; Gelin, M. F. *Physica A* **1996**, *229*, 501.

(9) H.-Contreras, M.; M.-Noyola, M.; V.-Rendon, A. *Physica A* **1996**, *234*, 271.

(10) Lukić, B.; Jeney, S.; Tischer, C.; Kulik, A. J.; Forró, L.; Florin, E.-L. *Phys. Rev. Let.* **2005**, *95*, 160601.

(11) Bard, A. J.; Faulkner, L. R. *Electrochemical Methods; Fundamentals and applications*; John Wiley & Sons: New York, 2001; pp 191−196.

(12) Aoki, K. *J. Electroanal. Chem.* **2006**, *592*, 31.

(13) (a) Bard, A. J.; Denuault, G. A.; Friesner, R. A. *Anal. Chem.* **1991**, *63*, 1282. (b) Unwin, P. R.; Bard, A. J. *J. Phys. Chem.* **1991**, *95*, 7814. (c) Unwin, P. R.; Mirkin, M. V.; Bard, A. J. *J. Phys. Chem.* **1992**, *96*, 4917. (d) Unwin, P. R.; Bard, A. J. *J. Phys. Chem.* **1992**, *96*, 5035. (e) Amphlett, J. A.; Denuault, G. *J. Phys. Chem. B* **1998**, *102*, 9946.

(14) Kwak, J.; Bard, A. J. *Anal. Chem.* **1989**, *61*, 1221.

(15) (a) Bard, A. J.; Crayston, J. A.; Kittlesen, G. P.; Shea, T. V.; Wrighton, M. S. *Anal. Chem.* **1986**, *58*, 2321. (b) Bard, A. J.; Shea, T. V. *Anal. Chem.* **1987**, *59*, 2101. (c) Fosset, B.; Amatore, C.; Bartelt, J.; Wightman, M. *Anal. Chem.* **1991**, *63*, 1403.

(16) Abramowitz, M.; Stegun, I. A. *Handbook of Mathematical Functions*, U.S. Government Printing Office: Washington, DC, 1972; combination of (29.3.49) at p 1024 with (29.2.15) at p 1021.

(17) Abramowitz, M.; Stegun, I. A. *Handbook of Mathematical Functions*, U.S. Government Printing Office: Washington, DC, 1972; (29.3.84) at p 1026.

(18) Hubbard, A. T.; Anson. F. C. In *Electroanalytical Chemistry*; Bard, A. J., Ed.; Marcel Dekker: New York, 1970; Vol. 4, p 156.

(19) Abramowitz, M.; Stegun, I. A. *Handbook of Mathematical Functions*, U.S. Government Printing Office: Washington, DC, 1972; (29.3.84) at p 378.

(20) Bard, A. J.; Faulkner, L. R. *Electrochemical Methods; Fundamentals and applications;* John Wiley & Sons: New York, 2001; p 353.

(21) Aoki, K.; Tanaka, M. *J. Electroanal. Chem.* **1989**, *266*, 11.

(22) Aoki, K.; Morita, M.; Niwa, O.; Tabei, H. *J. Electroanal. Chem.* **1988**, *256*, 269.

(23) Tanaka, N.; Tamamushi, R. *Electrochim. Acta* **1964**, *9*, 963.

(24) (a) Amatore, C.; Maisonhaute, E.; Simonneau, G. J. *Electroanal. Chem.* **2000**, *486*, 141. (b) Amatore, C.; Bouret, Y.; Maisonhaute, E.; Goldsmith, J. I.; Abruna, H. D. *Chem. Eur. J.* **2001**, *7*, 2206. (c) Amatore, C.; Bouret, Y.; Maisonhaute, E.; Abruna, H. D.; Goldsmith, J. I. *C. R. Chimie* **2003**, *6*, 99.

(25) Ikeuchi, H. *J. Electroanal. Chem.* **2005**, *577*, 55.